Energy levels and emission parameters of the Dy^{3+} ion doped into the YPO_4 host lattice

2009 J. Phys.: Condens. Matter 21 275501

(http://iopscience.iop.org/0953-8984/21/27/275501)

J. Phys.: Condens. Matter **21** (2009) 275501 (7pp) doi:10.1088/0953-8984/21/27/275501

Energy levels and emission parameters of the Dy^{3+} ion doped into the YPO_4 host lattice

R Faoro[1], F Moglia[1], M Tonelli[1], N Magnani[2] and E Cavalli[3]

[1] NEST, CNR-INFM and Dipartimento di Fisica, Università di Pisa, Largo Pontecorvo 3, 56127 Pisa, Italy
[2] European Commission, Joint Research Centre, Institute for Transuranium Elements, Postfach 2340, D-76125 Karlsruhe, Germany
[3] Dipartimento di Chimica Generale ed Inorganica, Chimica Analitica e Chimica Fisica, Università di Parma, via G. P. Usberti 17/a, 43100 Parma, Italy

E-mail: enrico.cavalli@unipr.it

Received 2 April 2009, in final form 30 April 2009
Published 10 June 2009
Online at stacks.iop.org/JPhysCM/21/275501

Abstract
Single crystals of Dy^{3+}-doped YPO_4 have been grown from $Pb_2P_2O_7$ flux and investigated by optical spectroscopy techniques. The energy level scheme of the active ion has been deduced from the low temperature spectra and reproduced by means of a crystal-field calculation. The room temperature absorption spectra have been analysed in the framework of the Judd–Ofelt approach, and the results of this analysis have been applied in a discussion concerning the spectral composition of the visible luminescence.

1. Introduction

The device potentialities of Dy^{3+}-based compounds strongly depend on the relative intensity of the blue ($^4F_{9/2} \rightarrow {}^6H_{15/2}$) and yellow ($^4F_{9/2} \rightarrow {}^6H_{13/2}$) emission channels. The yellow-to-blue intensity ratio (Y/B) of the Dy^{3+} luminescence was ascribed by Su *et al* [1] to different host related effects like covalency, site symmetry, etc, evidencing a rather complex dependence. We are exploring in detail the spectroscopic properties of a number of Dy^{3+}-doped materials in order to rationalize these effects [2–4]. This work is focused on Dy^{3+}-doped YPO_4 (YPO_4:Dy). Recent papers [5, 6] have indicated it as an attractive material for the development of efficient white phosphors. Moreover, since the emission properties of YPO_4:Dy are different to those of the isostructural YVO_4:Dy [7], the intensity ratio between the blue and the yellow emission can be conveniently modulated by varying the host composition of the $YP_xV_{1-x}O_4$:Dy (with $0 \leqslant x \leqslant 1$) solid solutions [8]. This possibility remarkably extends the application range of these materials. Despite these interesting perspectives, the electronic structures and luminescence dynamics of these compounds, and of YPO_4:Dy in particular, have not yet been investigated in detail. We then measured its polarized absorption and emission spectra and the fluorescence decay profiles as a function of the temperature and of the doping concentration. From the low temperature (LT) spectra we have deduced the complete energy level scheme of the Dy^{3+} ion in this host lattice and the observed energies have been fitted to a single-ion Hamiltonian containing free-ion and crystal-field interactions. The room temperature (RT) absorption spectra have been analysed in the framework of the Judd–Ofelt (JO) theory in order to obtain information about the efficiency of the radiative transitions and, in this particular case, about the branching ratios for the luminescence from the $^4F_{9/2}$ level, that regulate the relative intensities of the visible emission bands.

2. Experimental details

YPO_4 crystals doped with 0.5, 3 and 10% Dy (molar ratio with respect to Y) were grown by the 'flux growth' technique using $Pb_2P_2O_7$ as a solvent in the 1300–800 °C temperature range [9]. Their tetragonal structure was confirmed by means of single-crystal x-ray diffraction. In agreement with literature data, the space group is $I4_1/amd$ with $Z = 4$ [10, 11]. The cell parameters and the atomic coordinates are summarized in table 1. The Dy^{3+} doping ions enter the Y^{3+} sites having eightfold oxygen coordination and D_{2d} point symmetry. The

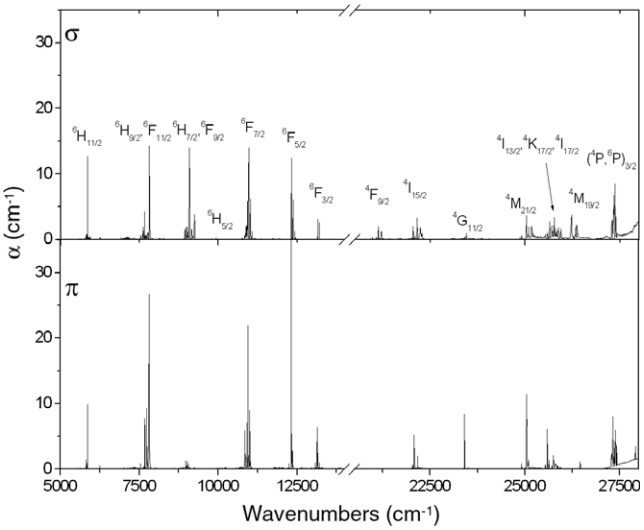

Figure 1. 10 K polarized absorption spectrum of YPO_4:Dy (3%).

Table 1. Cell parameters and atomic coordinates for YPO_4:Dy (3%).

	x/a	y/b	z/c
Y	0.000 00	0.750 00	0.125 00
P	0.000 00	0.250 00	0.375 00
O	0.000 00	0.074 93	0.215 68

Cell parameters (Å): $a = b = 6.894(2)$, $c = 6.293(2)$

zircon-type structure of the title compound can be described as built from chains of alternating edge-sharing PO_4 tetrahedra and YO_8 dodecahedra (bisdisphenoids) extending parallel to the crystallographic c axis and joined laterally by 'zigzag' chains parallel to the a axis.

The absorption spectra were recorded using a spectroscopic system made up of a 300 W halogen lamp fitted with a 0.22 Spex Minimate monochromator as source, and a 1.26 m Spex monochromator with an RCA C31034 photomultiplier or a PbS NEP cell for analysing and detecting the output radiation. The emission in the 470–670 nm range was excited at 390 nm using an UVLED (steady state measurements) or at 395 nm using the second harmonic of a pulsed Ti–sapphire laser (decay curve measurements). The luminescence signal was analysed by means of a Jobin-Yvon monochromator with 320 mm focal length and detected using a R1464 Hamamatsu photomultiplier. The crystals were mounted onto the cold finger of a He cryocooler and the measurements carried out at temperatures ranging from 10 to 298 K.

3. Low temperature spectra and crystal-field calculations

The 10 K polarized absorption spectrum of Dy^{3+} in YPO_4 is shown in figure 1. The observed multiplets, whose full widths at half-maximum (FWHM) are of the order of 15–20 cm^{-1}, correspond to the transitions from the $^6H_{15/2}$ ground state to the excited states of the $4f^9$ electronic configuration [12].

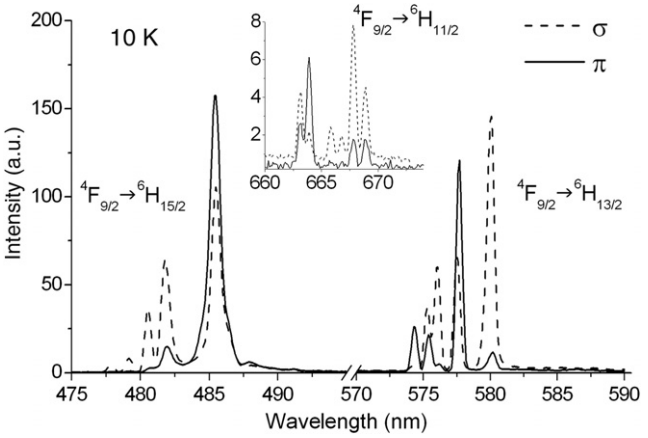

Figure 2. 10 K polarized emission spectrum of YPO_4:Dy (3%).

The number of the observed lines in some cases exceeds the $J + 1/2$ values expected from the crystal-field splitting of the $^{2S+1}L_J$ manifolds involved. This could be a consequence of the population, even at LT, of Stark components located just above the lowest level of the ground state or of the presence of minority centres, constituted for instance by Dy^{3+} ions located near to lattice defects. The Stark levels of Dy^{3+} are Kramers doublets and belong to the Γ_6 or Γ_7 double-group irreducible representations of the D_{2d} point group. The intensities of the optical transitions are regulated by the electric dipole selection rules:

$$E \parallel c \ (\pi \text{ polarization}) \qquad E \perp c \ (\sigma \text{ polarization})$$

$$\Gamma_6 \to \Gamma_7 \qquad \Gamma_6 \to \Gamma_{6,7}$$

$$\Gamma_7 \to \Gamma_6 \qquad \Gamma_7 \to \Gamma_{6,7}.$$

The structure of the ground state and of the first excited level can be obtained from the 10 K polarized visible emission spectra reported in figure 2. The three band systems centred at about 480, 575, 670 nm (inset) are assigned to the transitions from the $^4F_{9/2}$ excited level to the $^6H_{15/2}$, $^6H_{13/2}$ and $^6H_{11/2}$ levels respectively. The energy level scheme for the Dy^{3+} ion in YPO_4 deduced from the 10 K absorption and emission data is presented in table 2. The observed energies have been reproduced using the following RE Hamiltonian:

$$\hat{H} = \hat{H}_{\mathrm{FI}} + \hat{H}_{\mathrm{CF}} \tag{1}$$

where, according to [15], the free-ion part is written as

$$\hat{H}_{\mathrm{FI}} = E_{\mathrm{av}} + \sum_k F^k \hat{f}_k + \varsigma \hat{H}_{\mathrm{SO}} + \alpha L(L+1) + \beta \hat{G}(G_2) + \gamma \hat{G}(R_7) + \sum_i T^i \hat{t}_i + \sum_j M^j \hat{m}_j + \sum_k P^k \hat{p}_k \tag{2}$$

where $k = 2, 4, 6$; $i = 2, 3, 4, 6, 7, 8$; $j = 0, 2, 4$, and the crystal-field (CF) Hamiltonian for D_{2d} point symmetry is written as

$$\hat{H}_{\mathrm{CF}} = \sum_k \sum_q B_k^q \hat{C}_k^q = B_2^0 \hat{C}_2^0 + B_4^0 \hat{C}_4^0 + B_6^0 \hat{C}_6^0 + B_4^4(\hat{C}_4^4 + \hat{C}_4^{-4}) + B_6^4(\hat{C}_6^4 + \hat{C}_6^{-4}). \tag{3}$$

Table 2. Energy levels scheme of Dy^{3+} in YPO_4.

$^{2S+1}L_J$	Exp.	Calc.	Γ_n	$^{2S+1}L_J$	Exp.	Calc.	Γ_n
$^6H_{15/2}$	0	11	Γ_6	$^6H_{5/2}$	10 040	10 046	Γ_7
$(4\Gamma_6+4\Gamma_7)$	—	51	Γ_6	$(\Gamma_6+2\Gamma_7)$	10 121	10 119	Γ_6
	57	55	Γ_7		10 179	10 166	Γ_7
	117	124	Γ_6				
	173	175	Γ_7	$^6F_{7/2}$	10 853	10 879	Γ_7
	—	206	Γ_7	$(2\Gamma_6+2\Gamma_7)$	10 917	10 919	Γ_6
	—	283	Γ_7		10 952	10 945	Γ_7
	332	294	Γ_6		10 960	10 961	Γ_6
$^6H_{13/2}$	—	3466	Γ_7	$^6F_{5/2}$	12 254	12 269	Γ_7
$(3\Gamma_6+4\Gamma_7)$	3516	3506	Γ_7	$(\Gamma_6+2\Gamma_7)$	12 312	12 302	Γ_6
	3507	3509	Γ_6		12 319	12 317	Γ_7
	—	3552	Γ_7				
	3550	3553	Γ_6	$^6F_{3/2}$	13 094	13 089	Γ_6
	3619	3604	Γ_6	$(\Gamma_6+\Gamma_7)$	13 094	13 089	Γ_7
	3691	3608	Γ_7				
				$^6F_{1/2}$	13 642	13 625	Γ_6
$^6H_{11/2}$	5776	5772	Γ_6	(Γ_6)			
$(3\Gamma_6+3\Gamma_7)$	5814	5820	Γ_7				
	5819	5825	Γ_6	$^4F_{9/2}$	20 968	20 961	Γ_6
	5830	5841	Γ_7	$(3\Gamma_6+2\Gamma_7)$	21 070	21 073	Γ_6
	5848	5866	Γ_6		21 119	21 094	Γ_7
	5868	5899	Γ_7		21 146	21 155	Γ_6
					21 204	21 224	Γ_7
$^6H_{9/2}$	—	7516	Γ_6				
$(3\Gamma_6+2\Gamma_7)$	7541	7588	Γ_6	$^4I_{15/2}$	22 031	22 037	Γ_7
+	7600	7610	Γ_7	$(4\Gamma_6+4\Gamma_7)$	22 041	22 049	Γ_6
$^6F_{11/2}$	7626	7637	Γ_6		22 079	22 069	Γ_7
$(3\Gamma_6+3\Gamma_7)$	7682	7690	Γ_7		22 148	22 148	Γ_6
	7724	7722	Γ_6		22 172	22 166	Γ_7
	7746	7742	Γ_7		22 232	22 239	Γ_6
	7765	7766	Γ_6		-	22 255	Γ_7
	—	7766	Γ_7		22 276	22 279	Γ_6
	7814	7814	Γ_6				
	—	7858	Γ_7	$^4G_{11/2}$	23 359	23 355	Γ_7
				$(3\Gamma_6+3\Gamma_7)$	23 375	23 365	Γ_6
$^6H_{7/2}$	8937	8917	Γ_6		23 391	23 380	Γ_7
$(2\Gamma_6+2\Gamma_7)$	—	8932	Γ_7		23 397	23 382	Γ_6
+	8976	8997	Γ_7		23 409	23 433	Γ_7
$^6F_{9/2}$	9024	9027	Γ_6		23 446	23 454	Γ_6
$(3\Gamma_6+2\Gamma_7)$	9044	9037	Γ_6				
	9080	9081	Γ_6				
	—	9143	Γ_7				
	9153	9153	Γ_6				
	9241	9226	Γ_7				

This model Hamiltonian accounts for two-body electrostatic repulsion (F^k), two- and three-body configuration interactions (α, β, γ and T^i, respectively), spin–orbit coupling (ζ), spin–other-orbit interactions (M^j), electrostatically correlated spin–orbit interactions (P^k), and the crystal-field potential. A detailed description of the various free-ion operators and parameters is available in the literature [13]; the tensor operators $\hat{C}_k^q$ are defined in [14]. The CF parameters B_k^q are expressed according to the Wybourne normalization. Since $\hat{H}_{\mathrm{FI}}$ is expected not to change significantly when the same RE ion is embedded in different hosts, the free-ion parameters for Dy^{3+}–LaF_3 [15] were tentatively used as starting values, and some of them (F^2, F^4, F^6, ζ and α) were allowed to vary during the fitting procedure.

The irreducible representations reported in table 2 have been determined by calculation and associated with observed features according to their polarization behaviours. The best fit of the experimental data has been carried out using the free-ion parameters reported in table 3 and the CF parameters reported in table 4. The σ (rms) for this fit is 12 cm^{-1}, of the order of the experimental FWHM. The calculated energy levels are compared in table 2 with the experimental ones. The CF parameters (B_4^4 and B_6^4 in particular) of table 4 are to some extent different from those reported in a previous paper [7]: their final values depend in fact on the choice of the starting set, that can be made on the basis of literature data or of other evaluation criteria. In the present case, the reliability of the CF parameters has been tested by means of the superposition model (SPM) analysis, based on the main assumption that the crystal-field potential at the rare-earth site can be written as the sum of axially symmetric individual contributions [16] from the ligands. In this framework, the CF parameters can be

Table 3. Free-ion parameters for Dy^{3+} in YPO_4.

Parameters	Value (cm^{-1})
$E_{av.}$	55 859
F^2	90 807
F^4	64 579
F^6	49 035
ζ	1881
α	18.962
β	−633
γ	1790
T^2	329
T^3	36
T^4	127
T^6	−314
T^7	404
T^8	315
M^0	3.39
M^2	1.90
M^4	1.05
P^2	719
P^4	359
P^6	71.9

Table 4. CF parameters (cm^{-1}) for Dy^{3+} in YPO_4. The values determined by fitting the experimental energies are compared with those evaluated with the SPM.

	Fit	SPM
B_2^0	193 ± 12	(199)
B_4^0	247 ± 30	260
B_6^0	−867 ± 23	−1091
B_4^4	730 ± 21	675
B_6^4	132 ± 25	120

expressed as

$$B_n^m = N_n^m \langle r^n \rangle \sum_\ell \bar{A}_n(R_\ell) K_n^m(\theta_\ell, \varphi_\ell), \tag{4}$$

where K_n^m are the coordination factors defined in [17], ℓ labels the ligands, $\langle r^n \rangle$ is the average value of the nth power of the radius for the RE ion considered [18], N_n^m is a suitable numerical factor [19], and we have used the usual assumption that

$$\bar{A}_n(R_\ell) = \bar{A}_n(R_0)\left(\frac{R_0}{R_\ell}\right)^{t_n}. \tag{5}$$

Following the procedure described in [16] we have verified that the ratios B_n^4/B_n^0 are in qualitative agreement with the experiment: in fact, for $n = 4$ we obtain a ratio of about 2.6, practically independent of t_4 (to be compared with the experimental ratio 2.96), while for $n = 6$ its ratio is negative for $t_6 < 11$ (a reasonable assumption since in the pure point-charge model this exponent is 7) and close to the experimental value (−0.17) for t_6 between 1 and 3. Although overparametrization prevents attempting the same analysis for B_2^0 [20], we note that the latter parameter is predicted to be positive for YPO_4:Dy for all reasonable values of t_2.

The magnitude of the $\bar{A}_n$ parameters to be chosen is in line with literature estimates for zirconates [20]. The calculated crystal-field parameters are compared to the ones resulting from the fit in table 4.

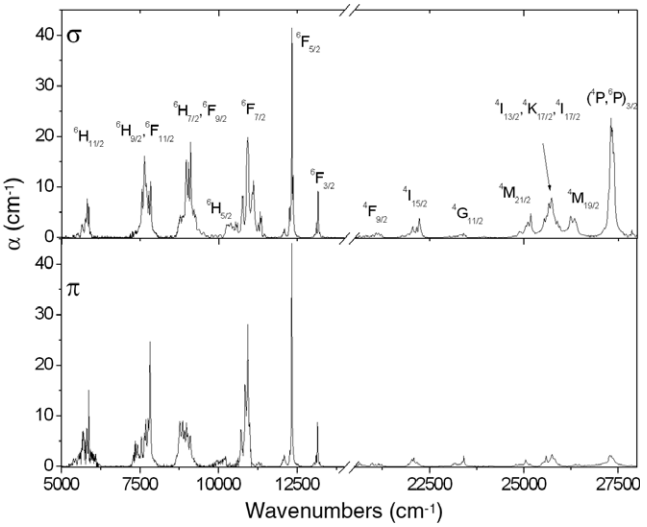

Figure 3. 298 K polarized absorption spectrum of YPO_4:Dy (3%).

4. Room temperature spectra and Judd–Ofelt analysis

The RT polarized spectrum of the title compound is shown in figure 3. In comparison with the LT spectrum, the number of components constituting the observed manifolds is increased, as well as their broadness.

Their intensities have been analysed in the framework of the Judd–Ofelt (JO) theory [21, 22]. Ten bands were considered to calculate the intensity parameters Ω_N ($N = 2, 4, 6$); we did not take into account the $^6F_{1/2} \leftarrow {}^6H_{15/2}$ transition because its intensity is negligible. The oscillator strengths of the transitions were determined by considering the polarization of the bands with a 2:1 ratio for σ:π, and the experimental data were fitted on the basis of the JO parametrization scheme after subtraction of the magnetic dipole contribution for the $^4I_{15/2} \leftarrow {}^6H_{15/2}$ transition. This contribution is small and not reported here. The reduced matrix elements were taken from Jayasankar and Rukmini [23], and the value of the refractive index was assumed to be $n = 1.75$ according to Zheng *et al* [24]. The evaluated intensity parameters, the observed and calculated oscillator strengths, the root mean square deviation (RMS) and the per cent error are reported in table 5.

These parameters have been used for the calculation of the spontaneous emission probabilities and of the radiative branching ratios for the transitions from the $^4F_{9/2}$ state to the lower ones, which are reported in table 6 together with the radiative lifetime of the emitting level.

In table 7(a) these results are compared with those obtained for YVO_4:Dy [7]: it can be noted that the ratio between the branching ratio for the yellow and blue emission is much larger for the latter than for the former crystal. The Ω_2 parameter is much larger for the vanadate than the phosphate crystal, as an effect of the major intensity, in the former, of the hypersensitive $^6F_{11/2} \leftarrow {}^6H_{15/2}$ absorption transition, whose reduced matrix elements are listed in table 7(b) together with those related to the blue and yellow emission transitions. It has to be pointed out that these are not

Table 5. Experimental and calculated oscillator strengths (P) of Dy^{3+} in YPO_4. The Judd–Ofelt parameters, Ω_λ, the RMS and the per cent error are also tabulated.

Excited state	Barycentre (cm^{-1})	P_{exp} (10^6)	P_{calc} (10^6)
$^6H_{11/2}$	5 763	1.04	1.24
$^6H_{9/2} + {}^6F_{11/2}$	7 667	2.78	2.75
$^6H_{7/2} + {}^6F_{9/2}$	8 981	3.13	3.25
$^6F_{7/2}$	11 090	3.33	2.83
$^6F_{5/2}$	12 322	1.35	1.35
$^6F_{3/2}$	13 138	0.32	0.25
$^4F_{9/2}$	20 962	0.20	0.21
$^4I_{15/2}$	22 094	0.34	0.47
$\Omega_2 = 0.51 \times 10^{-20}$ cm^2, $\Omega_4 = 1.91 \times 10^{-20}$ cm^2, $\Omega_6 = 2.87 \times 10^{-20}$ cm^2			
RMS $= 2.58 \times 10^{-7}$; error 16.5%			

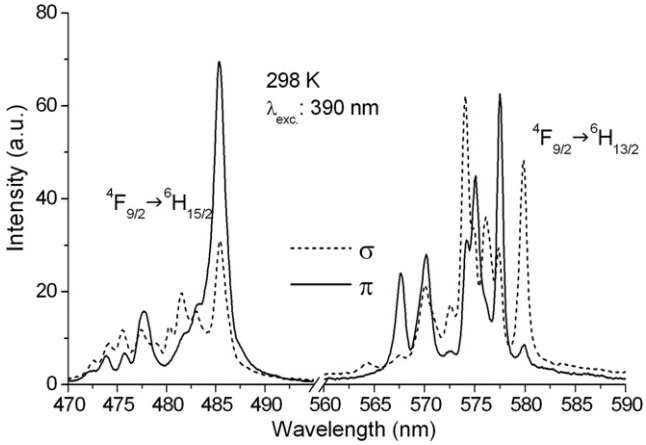

Figure 4. 298 K polarized emission spectrum of YPO_4:Dy (3%).

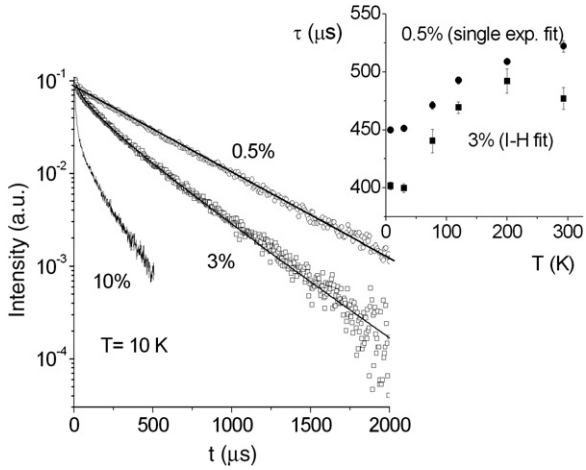

Figure 5. 10 K emission decay profiles of differently concentrated YPO_4:Dy crystals. In the inset the temperature dependences of the decay times are shown (see the text).

Table 6. Calculated spontaneous emission probabilities A and radiative branching ratios β for the $^4F_{9/2}$ emitting level.

Final state	A (s^{-1})	β
$^6F_{5/2}$	1	0.002
$^6F_{7/2}$	6	0.007
$^6H_{5/2}$	4	0.006
$^6H_{7/2}$	0	0
$^6F_{9/2}$	7	0.009
$^6F_{11/2}$	12	0.016
$^6H_{9/2}$	13	0.016
$^6H_{11/2}$	22	0.029
$^6H_{13/2}$	412	0.528
$^6H_{15/2}$	303	0.388
Radiative lifetime $\tau = 1279$ μs		

hypersensitive transitions, as erroneously claimed in some papers [5, 6, 8]; however their intensities are strongly affected by the Ω_2 and Ω_4 JO parameters. For large values of these parameters in fact we have to expect a relatively strong visible luminescence spectrum dominated by the yellow component, whereas with Ω_2 and Ω_4 decreasing the overall emission should concomitantly decrease with the intensity of the blue band progressively approaching, but never exceeding, that of the yellow one.

The experimental trend observed in [8] (figure 5(a)) for the $Y_{0.99}Dy_{0.01}P_xV_{1-x}O_4$ ($0 \leqslant x \leqslant 1$) compositions is in reasonable agreement with this model. The 298 K polarized emission spectrum of Dy:YPO_4 in the 470–590 nm region (figure 4) is composed of two band systems having comparable intensity, in agreement with the low values of Ω_2 and Ω_4.

5. Excited states dynamics

The decay profile of the $^4F_{9/2}$ emission has been measured as a function of the temperature and of the Dy^{3+} concentration. The 10 K curves are shown in figure 5. In the case of the 0.5% doped crystal, the observed behaviour is a single exponential with decay time of 450 μs. The average distance between two active ions in this case is rather long, about 15 Å, allowing us to exclude the possibility of efficient energy transfer processes. As for a number of Dy^{3+}-doped materials [2, 3, 25], with the temperature increasing the decay time increases from 450 up to 520 μs at 298 K (see the inset of figure 5). This value is significantly shorter than the radiative lifetime estimated by the JO method (1279 μs), and the difference is too important to be ascribed to non-radiative processes. Analogous behaviour has already been observed in the case of Dy:YSGG [26] and Dy:BYF [4]: in our opinion, low values of the Ω_2 intensity parameter result in the overestimation of the calculated radiative lifetime. The reason for this apparent anomaly of the JO model has not yet been clarified. At present

Table 7. (a) Comparison between the intensity parameters, the radiative lifetime of $^4F_{9/2}$ and the calculated $\beta_{^6H_{13/2}}/\beta_{^6H_{15/2}}$ (Y/B) ratio in the YPO_4 and YVO_4 host lattices. (b) Reduced matrix elements for some relevant absorption and emission transitions (from [23]).

(a)	Ω_2 ($\times 10^{20}$ cm^2)	Ω_4 ($\times 10^{20}$ cm^2)	Ω_6 ($\times 10^{20}$ cm^2)	τ (μs) (Y/B)
YPO_4	0.51	1.91	2.87	1279 (1.36)
YVO_4	6.59	3.71	1.74	440 (4.13)
(b)	$\|U^2\|^2$	$\|U^4\|^2$	$\|U^6\|^2$	
$^6F_{11/2} \leftarrow {}^6H_{15/2}$	0.9349	0.8310	0.2002	Absorption
$^4F_{9/2} \rightarrow {}^6H_{15/2}$	0.0	0.0049	0.0303	Blue emission
$^4F_{9/2} \rightarrow {}^6H_{13/2}$	0.0512	0.0172	0.0573	Yellow emission

we are collecting new experimental data in order to reveal systematic trends useful in understanding the origin of this effect. The decay curves of the 3% doped compound are not exponential, indicating the occurrence of energy transfer processes.

The Inokuti–Hirayama (IH) model for the energy transfer in the absence of migration [27] can be reliably applied to the fit of the emission profiles:

$$I(t) = I_0 \exp\left[-\frac{t}{\tau} - \alpha\left(\frac{t}{\tau}\right)^{\frac{3}{s}}\right]. \quad (6)$$

$I(t)$ is the emission intensity after pulsed excitation, I_0 is the intensity of the emission at $t = 0$, τ is the lifetime of the isolated donor, α is a parameter containing the energy transfer probability and $s = 6$ for dipole–dipole (D–D), 8 for dipole–quadrupole (D–Q) and 10 for quadrupole–quadrupole (Q–Q) interaction. In the present case the best fit of the experimental data has been obtained with $s = 10$. The resulting decay time ranges from about 400 μs at 10 K to about 480 μs at 298 K, in reasonable agreement with the diluted case (see the inset of figure 5). The parameter α is defined as follows:

$$\alpha = \frac{4}{3}\pi\Gamma\left(1 - \frac{3}{s}\right)N_a R_0^3 \quad (7)$$

where Γ is the gamma function, N_a the concentration of the acceptor expressed in ions cm^{-3} and R_0 is the critical distance, that in this case ranges from 7.3 to 8 Å, in good agreement with the calculated average distance between the Dy^{3+} ions, $d_{Dy-Dy} = 8$ Å. When the Dy^{3+} concentration rises to 10% ($d_{Dy-Dy} = 5.5$ Å) the decay becomes strongly non-exponential (figure 5) probably as an effect of migration processes that give rise to a significant concentration quenching. As a result, the long time tail of the profile still evidences a single-exponential behaviour, with a decay constant (of the order of 130 μs) much shorter than in the previous cases.

6. Concluding remarks

The structure of the Stark levels of Dy^{3+} in YPO_4 has been determined on the basis of the low temperature optical spectra and reproduced by a CF calculation. The reliability of the calculated CF parameters has been confirmed by means of the SPM analysis. The host dependence of the yellow-to-blue intensity ratio (Y/B) of the Dy^{3+} luminescence has been discussed in the light of the results of the Judd–Ofelt analysis, demonstrating that the Y/B intensity ratio directly depends on the values of the Ω_2, and to a lesser extent, Ω_4 intensity parameters and that low values of these parameters imply some inconsistency between the experimental and the calculated lifetime of the $^4F_{9/2}$ state. The concentration behaviour of the decay profiles has evidenced energy transfer processes taking place for doping levels exceeding the 1% value. We are extending the investigations to other Dy^{3+}-based materials in order to test the correctness of the above conclusions and their applicability in the development of new phosphors.

Acknowledgments

This work was financially supported by MIUR (Italian Ministry of University and Scientific Research—PRIN2007 project). N Magnani acknowledges the European Commission for support given in the framework of the programme 'Training and Mobility of Researchers'.

References

[1] Su Q, Pei Z, Chi L, Zhang H, Zhang Z and Zou F 1993 *J. Alloys Compounds* **192** 25
[2] Cavalli E, Bovero E and Belletti A 2002 *J. Phys.: Condens. Matter* **14** 5221
[3] Cavalli E, Bovero E, Magnani N, Ramirez M O, Speghini A and Bettinelli M 2003 *J. Phys.: Condens. Matter* **15** 1047
[4] Parisi D, Toncelli A, Tonelli M, Cavalli E, Bovero E and Belletti A 2005 *J. Phys.: Condens. Matter* **17** 2783
[5] Xiu Z, Yang Z, Lü M, Liu S, Zhang H and Zhou G 2006 *Opt. Mater.* **29** 431
[6] Lai H, Bao A, Yang Y, Xu W, Tao Y and Yang H 2008 *J. Lumin.* **128** 521
[7] Cavalli E, Bettinelli M, Belletti A and Speghini A 2002 *J. Alloys Compounds* **341** 107
[8] Bao A, Yang H, Tao C, Zhang Y and Han L 2008 *J. Lumin.* **128** 60
[9] Smith S H and Wanklyn B M 1974 *J. Cryst. Growth* **21** 23
[10] Milligan W O, Mullica D F, Beall G W and Boatner L A 1982 *Inorg. Chim. Acta* **60** 39
[11] Chakoumakos B C, Abraham M M and Boatner L A 1994 *J. Solid State Chem.* **109** 197
[12] Kaminskii A A 1996 *Crystalline Lasers: Physical Processes and Operating Schemes* (Boca Raton, FL: CRC Press)
[13] Crosswhite H M and Crosswhite H 1984 *J. Opt. Soc. Am.* B **1** 246 and references therein
[14] Racah G 1942 *Phys. Rev.* **62** 438

[15] Carnall W T, Goodman G L, Rajnak K and Rana R S 1989 *J. Chem. Phys.* **90** 3443
[16] Newman D J and Ng B 1989 *Rep. Prog. Phys.* **52** 699
[17] Newman D J 1971 *Adv. Phys.* **20** 197
[18] Freeman A J and Desclaux J P 1979 *J. Magn. Mater.* **12** 11
[19] Weber M J and Bierig R W 1964 *Phys. Rev.* **134** A1492
[20] Newman D J and Ng B 2000 *Crystal Field Handbook* (Cambridge: Cambridge University Press)
[21] Judd B R 1962 *Phys. Rev.* **127** 750
[22] Ofelt G S 1962 *J. Chem. Phys.* **37** 511
[23] Jayasankar C K and Rukmini E 1997 *Physica* B **240** 273
[24] Zheng H and Meltzer R S 2007 *J. Lumin.* **122/123** 478
[25] Kaminskii A A, Gruber J B, Bagaev S N, Ueda K, Hömmerich U, Seo J T, Temple D, Zandi B, Kornienko A A, Dunina E B, Pavlyuk A A, Klevtsova R F and Kuznetsov F A 2002 *Phys. Rev.* B **65** 125108
[26] Sardar D K, Bradley W M, Yow R M, Gruber J B and Zandi B 2004 *J. Lumin.* **106** 195
[27] Inokuti M and Hirayama F 1965 *J. Chem. Phys.* **43** 1978